Desalination and nutrient removal from tertiary treated urban wastewater by a radial capacitive deionizer

Ricardo Franci Gonçalves[1], Constansa Valadares Tripoli[2], Patrick Curran[3]

[1] Federal University of Espírito Santo, Department in Environmental Engineering, Av. Fernando Ferrari, 514, Goiabeiras, 29075-910, Vitória, Espírito Santo, Brazil.

[2] Sanefort Environmental Equipment Solutions

[3] Atlantis Technologies

Desalination and nutrient removal from tertiary treated urban wastewater by a radial capacitive deionizer

Abstract

This study focused on removing salts and nutrients (nitrogen and phosphorus) from tertiary treated urban wastewater by capacitive deionization. The performance of a pilot-scale radial capacitive deionizer subjected to varying feed flow rates during the purification stage and constant flow rates during the reject stage was evaluated. This operational strategy aimed to maximize the water recovery rates of the system, with electrical adjustments being made proportionally to the water recovery rate. Lower hydraulic loads resulted in the radial capacitive deionizer removing more ions from the sewage, albeit with higher specific energy consumption. Optimal operational conditions reduced conductivity by 92.8%, with a specific energy consumption of 2.17 $kWh.m^{-3}$. Significant removals of ammonium, nitrite, nitrate, and orthophosphate ions were observed, with average specie reductions of up to 84, 91.4, 100, and 60.5%, respectively. Higher rates of treated water recovery resulted in lower ion removal reduction and energy consumption. The limiting step of the process referred to ion desorption, requiring the correct adjustment of the time lapse, flow rate, and applied electrical voltage to ensure the efficiency of the subsequent purification stage. A loss of efficiency was observed when the process was run continuously, thus emphasizing the strategic significance of capacitor rinsing during the rejection phase across multiple subsequent treatment cycles.

Keywords

Urban wastewater, desalination, nutrient removal, capacitive deionization, operational parameters.

1. Introduction

Capacitive deionization (CDI) has been gaining increasing interest in the production of demineralized water from low-salinity waters (Tsai et al., 2021; Maheshwari, Agarwal & Solanki, 2020). This electrochemical treatment aims to remove charged chemical species dissolved in aqueous solutions. A CDI cell consists of a pair of porous electrodes usually made of carbon kept at a small distance apart by a spacer with a cationic membrane in between the spacer and the electrode and an anionic membrane in between the spacer and the other electrode. Feedwater flows through the spacer or flow channel and with the cell operating at 1 to 1.4 V. During this process, the ions in the liquid migrate through the respective membrane to the electric double layers on the porous electrode surface and are removed by electrosorption. The adsorbed ions are released from the partially saturated electrode by reversing or reducing the polarity of the system, releasing the electrostatically retained ions in a highly concentrated liquid stream (SUSS et al., 2015).

The performance of a CDI system depends on various operational characteristics and system compositions. The electrode surface area and material, pore size, applied electrical potential, inlet flowrate, and the physicochemical properties of the liquid to be treated are crucial factors for CDI performance (SHUI; ALHSEINAT, 2019). Operational parameters such as hydraulic load and the configuration of the ion adsorption and desorption cycles also directly influence CDI efficiency in desalinating waters (Guyes et al., 2021). Decreasing the hydraulic load increases the residence time of the fluid inside the cell and the electrosorption time of ions by the electrodes (Ntakirutimana et al., 2020). However, the time water remains in contact with the electrodes inside the cells must be balanced to maintain electrosorption at acceptable levels (PORADA et al., 2012). Excessively long electrosorptions can saturate electrodes and increase salt concentrations in the effluent. The interaction time between ions and electrodes in CDIs operating with continuous feed and single-pass flow is defined by the hydraulic load

applied to the process (CHUNG, 2018). According to Salari et al. (2022), CDIs operating in batch mode favor lower hydraulic loads to ensure effective electrosorption. However, excessively low hydraulic loads tend to create dead zones between the electrodes, compromising the performance of the system (TANG et al., 2015).

Another determining factor in CDI desalination refers to feedwater composition. The selectivity of deionization in multi-solvent solutions is determined by several physicochemical properties of ions, including charge, radius, and concentration of each ion in the solution (Chai et al., 2022). Divalent ions are more effectively removed than monovalent ions due to their electric charge. In solutions with ions of the same charge, the ion with a smaller ionic radius is preferentially adsorbed over the ion with a larger ionic radius (Tsai et al., 2021). Moreover, the molar concentration of ions in a solution plays an important role in their selectivity in an electrochemically competitive environment. However, the solute concentrations should be associated with the size of ions in the solution and the average pore size of the electrodes. Electrodes with pores smaller than the size of a ion hinder adsorption (HOU; HUANG, 2013; NOKED et al., 2010).

Tsai et al. (2021) and Maheshwari, Agarwal & Solanki (2020) describe the good efficiency of capacitive deionization in producing demineralized water from known saline waters. However, its applicability as an advanced treatment alternative for tertiary-treated sanitary wastewater generates controversies, especially due to its complex composition and small concentrations of organic matter. Nevertheless, its advantages over reverse osmosis in low-salinity waters (<3000 mS/cm) support the high interest in the technology. Its main advantages over reverse osmosis are its low energy consumption and high factor of treated water recovery.

As it is a relatively new technology, the literature has few studies on its operational performance in wastewater treatment. Ramachandran et al. (2019) evaluated the effect of applying reduced hydraulic loads during the reject cycle, observing improvements in water recovery rates. They achieved recovery rates of around 90% compared to the commonly obtained 50% with conventional constant flow operation. Rommerskirchen et al. (2020) described similar results in the capacitive deionization of waters with 60 and 120 g/L NaCl concentrations, with water recovery rates ranging from 70 to 92%, respectively. Zhang et al. (2020) obtained good water recovery rates, reaching values of up to 92%. However, the authors noted that shorter reject steps (higher WR) resulted in the progressive accumulation of ions on the electrodes.

This study aimed to investigate the efficiency and ion selectivity of a radial capacitive deionizer (RDI) in treating an effluent from an activated sludge treatment plant, evaluating the effects of different operational strategies on RDI advanced treatment efficiency and energy consumption. This research tested various operational strategies by varying the hydraulic load and the configuration of the adsorption/desorption cycle to maximize water recovery with a high-quality standard and low energy density.

2. Material and methods

This research was conducted at Sewage Treatment Plant facilities, which consists of an NPBR activated sludge system that can treat a 400 $L.s^{-1}$ average flow rate. Before feeding the CDI, the effluent from this wastewater treatment plant (WWTP) underwent tertiary treatment that consisted of (Figure 1):

Submerged aerated biofilter: with a total height of 3.20 m, a diameter of 1.20 m, and a support bed height of 2.4 m. The support bed had a total volume of 2.71 m^3, a specific surface area of 450 $m3.m^{-2}$, and was composed of a mixture of polyethylene rings (d = 25 mm and L = 25 mm)

and polystyrene beads with D = 2.2 mm. The average superficial aeration rate was 12 $m^3.m^{-2}.h^{-1}$, and the average volumetric organic loading rate was 1.1 $Kg.m^{-3}.d^{-1}$.

Sand filter: a polyethylene filter with a diameter of 35 cm. a total height of 79 cm, and a sand granulometry ranging from 0.7 to 1.7 mm. The average superficial hydraulic loading rate applied to the filter was 24.4 $m^3.m^{-2}.h^{-1}$.

Activated carbon (AC) filter: a polyethylene filter with a diameter of 35 cm, a total height of 79 cm, and an AC granulometry ranging from 2.4 to 2.9 mm. The average superficial hydraulic loading rate applied to the filter was 24.4 $m^3.m^{-2}.h^{-1}$.

Equalization tank: a polyethylene reservoir with a volume of 500 L and a hydraulic detention time ranging from 0.60 to 1.39 hours.

The submerged aerated biofilter served to additionally remove SS and BOD from the secondary effluent and elevate its redox potential above 320 mV (Ag/AgCl). The sand filter aimed to provide additional SS removal and the activated carbon filter facilitated the adsorption of organic compounds that may damage membranes and electrodes. The purified water, reject water, and cylinder-cleaning water from the RDI were directed to different reservoirs.

Figure 1 - View of the experimental apparatus: post-treatment [submerged aerated biofilter, sand filter, charcoal filter, cartridge filter, and radial capacitive deionizer (RDI)].

2.1. Radial Capacitive Deionization Equipment

A capacitive deionization equipment, model S-25, developed by Atlantis Technologies (Figure 2), was used in this study. It consists of multiple cylinders filled with supercapacitors operating under a constant electric current. These cylinders can be operated in series or in parallel depending on the defined operational strategy. The equipment includes a control system for inlet, cleaning, and reject flows, and automatic data logging for variables such as flow rate, voltage, current, and conductivity. Operational routines can be configured with parameters

such as stage name, stage execution time, applied voltage, pump speed, state of solenoid valves, power supply, applied polarity, and pump operation status. The system also includes general control parameters such as data logging frequency, pressure limit points, and repetition of the selected operational protocol.

The equipment includes the following components:

- Electrical Control Panel with a power supply switch, circuit breakers, and a programmable logic controller (PLC).
- DI Cylinders: Six cylinders that can operate hydraulically in parallel or series.
- A constant voltage power supply with automatically reversible polarity.
- A Procon Series 3 125GPH Inox 316 positive displacement rotary vane pump.
- Polypropylene filter (Height = 594 mm and D = 184 mm) with a filtration grade of 5 mm.
- Human-Machine Interface (HMI).
- Specific sensors: electrical conductivity, pressure, and flow.
- Solenoid and pressure relief valves.
- Hydraulic circuits: feed, purified, reject, and recycle.

2.2. Configuration of the Capacitive Deionizer

Each RDI cylinder consists of two electrode/membrane sets, each with a width of 0.33 m and a length of 15.2 m, totaling 20 m^2 of surface area and 6 L of useful volume (Figures 3-1 and 3-2). A double-layer device (1002) comprising a first (102) and a second capacitors (104) forms a cylindrical spiral with an axis centrally arranged around a water-impermeable mandrel on which the two capacitors are wound (200). Electrodes 1 and 6 are coated with anion exchange membranes, whereas electrodes 3 and 4 are coated with cation exchange membranes. The electrode and semipermeable membrane sets are separated by a dielectric spacer with an approximate thickness of 400 microns, forming the hydraulic flow path in the axial direction of the cylinder. The electrodes are enveloped by either cationic or anionic semipermeable membranes, preventing discharged ions from being reabsorbed into the electrodes of the opposite capacitor when the polarities of the capacitors are reversed for rejection.

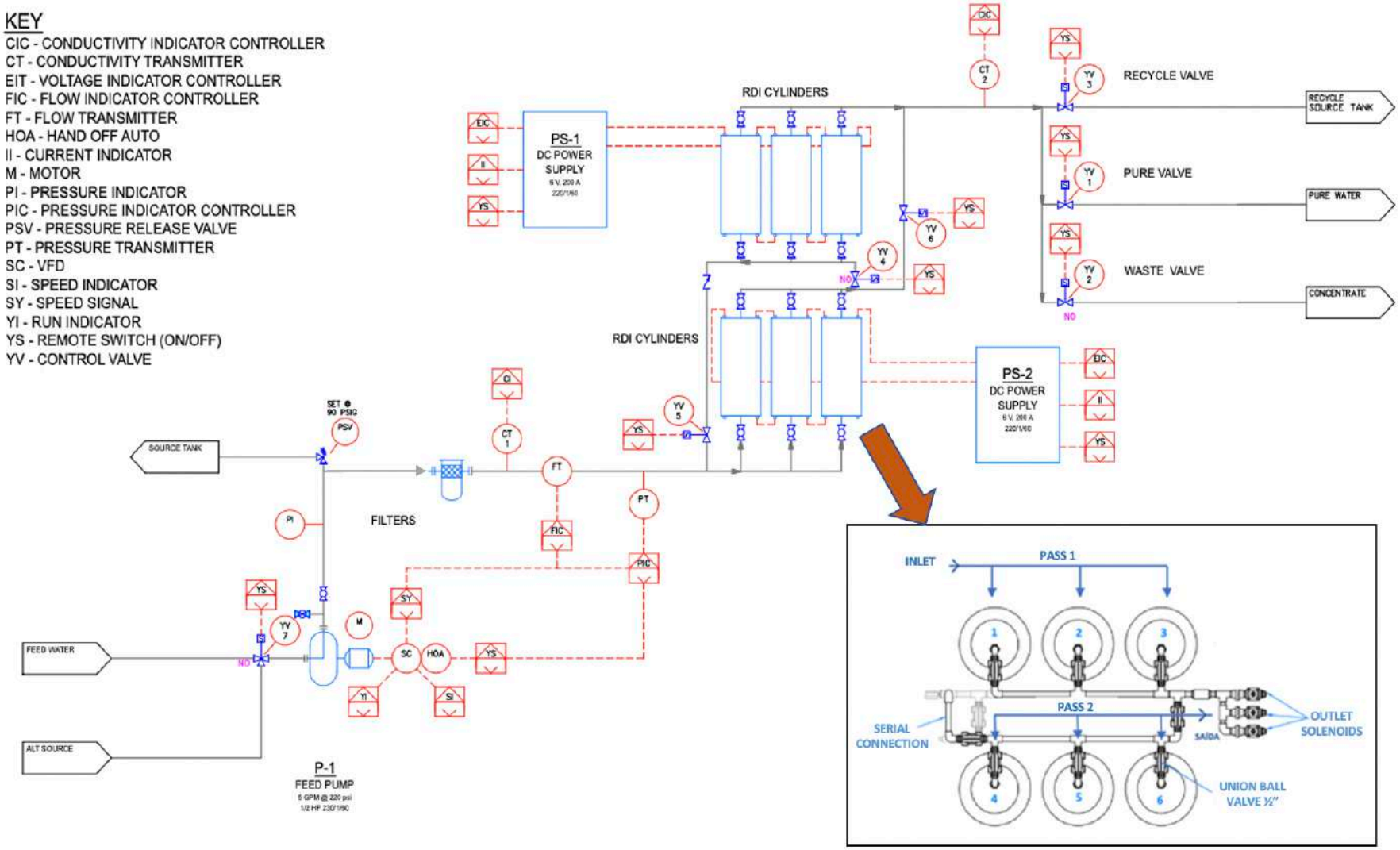

Figure 2 - Process and instrumentation diagram of the RDI S-10 equipment (Source: Adapted from Atlantis Technologies, 2020)

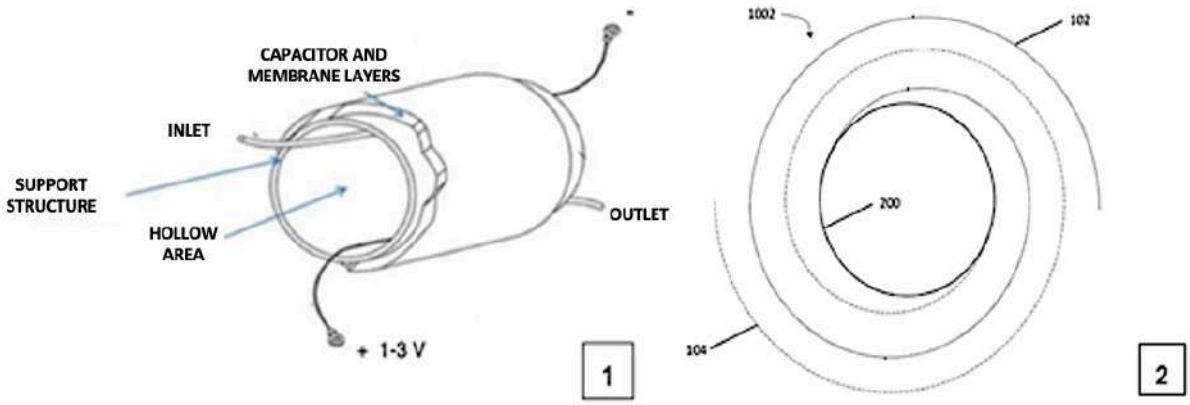

Figure 3 - Sketch of the RDI equipped with two double-layer capacitors.

The RDI operates intermittently under a treatment cycle consisting of three distinct stages: purification, regeneration (reject), and system cleaning. In the purification stage, a positive voltage is applied across the positive and negative electrodes, creating an electric field within the cylinders. As a result, anions are attracted to the positive electrode, and cations are attracted to the negative electrode. The ions are retained in their respective electrodes and purified water flows through the spacers. The system operates in constant voltage mode as the applied current is monitored. A decrease in the applied current indicates that the capacitors are approaching their maximum ion adsorption capacity, signaling that the device should enter reject mode.

The first two reject stages involve desorbing ions from the electrodes. During this phase, a negative voltage is applied to the electrodes (i.e., the polarity of the applied voltage to the electrodes is reversed), repelling the ions and creating a reject water flow. To improve water recovery rates, the first reject stage is performed without flow inside the cylinder, causing the ions to desorb into the liquid within it without generating a reject current. The third stage cleans the pipeline and the interior of the cylinder in preparation for the start of the subsequent treatment cycle (Table 1).

Table 1 - Stages of the treatment cycle

Treatment Cycle Steps	Polarity	Direction of Flow	System Setup
Purification	Positive	Purified water stream	
Reject - Zero Flow	Inverted	-	Two cylinders in series
Reject	Inverted	Reject stream	
System Cleaning	Positive	Reject stream	

In this study, the RDI was operated under the batch method, in which the tertiary effluent was pumped from the inlet reservoir and directed to the respective outlet reservoirs. Thus, the treated water passed through the device only once instead of being continuously recycled. The strategy of applying constant voltage and monitoring the applied current was adopted. A decrease in the applied current indicates that the capacitors are approaching their maximum

ion adsorption capacity, signaling that the device should enter reject mode to regenerate the capacitors. This research was conducted in two stages:

1st stage - Evaluation of RDI desalination performance and efficiency based on salt removal efficiency (%), specific energy consumption, and water recovery rates.

2nd stage - Evaluation of RDI efficiency in removing different ionic compounds based on the three scenarios that best removed salinity in the first stage.

1st stage: The experiments involved variations in hydraulic loads during the purification stage, followed by a decrease in flow during the reject stage. The control variables (applied voltage and flow rate) were optimized to maximize desalination. The aim was to maximize recovery in a continuous flow treatment cycle operating in batches. Additionally, the impact of varying hydraulic loads on specific RDI energy consumption was evaluated. Operational scenarios were developed by applying five flow rates during the purification stage and three water recovery rates, with electrical adjustments made as water recovery rates increased. Thus, a total of 15 operational scenarios were generated. All tests were performed in triplicates. Before starting the first repetition of the treatment cycle, the system was cleaned following the same configuration as the system cleaning step imposed in the scenarios with 70 and 80% water recovery rate: a 6 $L.min^{-1}$flow rate, a 1-minute time lapse, and a 5.3V voltage (Table 2).

Table 2 - Tested conditions in the first stage of the research

Operating parameters	Tested conditions
Flow rate ($L.min^{-1}$)	6, 8, 10, 12, and 14
Water recovery rate (%)	70, 80, and 90
Voltage (V)	5.3, 5.6, and 5.9

2nd stage: The second experiment aimed to evaluate how efficiently the RDI removed the ionic compounds NH^{4+}, NO^{2-}, NO^{3-}, and PO_4^{3-} based on the three scenarios that obtained the best desalination results in the first stage: phases 1, 4, and 7 (Table 3). These phases had a water recovery rate of 70% under a 5.3V voltage. The only control variable in the second stage of testing was the hydraulic load applied in each scenario, which proportionally altered the organic and ionic loads on the RDI (Table 2).

Table 3 - Operational parameters of the tested scenarios and their impacts on the RDI performance (n = 5)

	PURIFIED - PHASE 1				PURIFIED - PHASE 4				PURIFIED - PHASE 7			
OPERATING PARAMETERS	Median (SD)	Minimun	Maximum	Coefficient of variation (CV)	Median (SD)	Minimun	Maximum	Coefficient of variation (CV)	Median (SD)	Minimun	Maximum	Coefficient of variation (CV)
Flow rate ($L.min^{-1}$)	5.8 ± 0.1	5.7	5.9	1%	7.9 ± 0.1	7.7	8.0	1%	9.8 ± 0.1	9.7	10.0	1%
Hydraulic load ($m^3.m^{-2}.h^{-1}$)	28.9 ± 0.4	28.6	29.5	1%	39.2 ± 0.5	38.7	40.0	1%	48.8 ± 0.5	48.5	49.8	1%
Specific energy consumption ($kWhr.m^{-3}$)	1.8 ± 0.1	1.5	1.9	8%	1.5 ± 0.1	1.3	1.5	8%	1.3 ± 0.1	1.1	1.4	9%
Conductivity reduction efficiency (%)	84.2 ± 0.1	79.2	91.0	6%	77 ± 0.1	71.2	87.9	9%	73.3 ± 0.1	65.9	86.1	11%
Water recovery rate (%)	70 ± 0.3	70.2	70.9	0%	70 ± 0.3	69.6	70.3	0%	70 ± 0.3	69.7	70.6	0%

2.3. Evaluation of RDI Performance

The performance of the RDI system was assessed by its ion removal efficiency, volumetric energy consumption, water recovery rate, and applied hydraulic load. The variables used in the calculations included flow rate, inlet and outlet conductivity, voltage, and electric current.

The average ion removal efficiency and water recovery rate were calculated using equations 1 and 2, respectively.

$$Efficiency\ (\%) = \frac{(C_{in} - C_{out})}{C_{in}} \times 100 \qquad (1)$$

Where:
Reduction - Percentage of ion removal from the treated liquid (%);
Cin - Average ion concentration at the RDI inlet ($mg.L^{-1}$);
Cout - Average ion concentration at the RDI outlet ($mg.L^{-1}$).

$$WR\ (\%) = \frac{V_{purified}}{V_{reject} + V_{purified}} \qquad (2)$$

Where:
WR - Ratio of purified water volume to the total water volume (sum of purified water and reject volume in the cycle) (%);
Vreject - Volume of water produced during the reject and system cleaning stages (L);
Vpurified - Volume of water produced during the purification stage of the cycle (L).

The specific energy consumption per unit volume (Ev) and the volumetric hydraulic load were calculated using equations 3 and 4, respectively.

$$SEC = \frac{EC}{V} \qquad (3)$$

Where:
SEC - Specific energy consumption per unit volume ($kWh.m^{-3}$ of treated water);
EC - Energy consumption in the treatment cycle (kWh);
V - Volume of treated water in the cycle (m^3 of treated water).

$$VHL = \frac{Q}{V} \qquad (4)$$

Where:
VHL - Volumetric Hydraulic Load ($m^3.m^{-3}.h^{-1}$);
Q - Inlet flow rate to RDI ($m^3.h^{-1}$);
V - RDI useful volume (reactive volume) (m^3).

2.4. Physicochemical analysis of influent and effluent from RDI

The flows of tertiary effluent and purified water, reject water, and system cleaning streams were stored entirely in their respective reservoirs during each operation cycle of the RDI. To collect the composite samples, the volume stored in each reservoir was previously homogenized. After each treatment cycle, the water outlet reservoirs were cleaned for subsequent storage. The tertiary effluent, submerged aerated biofilter, sand filter, activated carbon filter, and equalization tank samples were always collected in the morning from 8 a.m. to 12 p.m. All samples were collected in 1000 ml polyethylene bottles and preserved at 4°C. Depending on the compound to be determined, the sample was preserved by adding sulfuric acid to achieve a pH below 2. The following laboratory analyses were performed according to APHA (2012): temperature, pH, turbidity, conductivity, dissolved oxygen, total dissolved solids, total alkalinity, chemical oxygen demand, $N\text{-}NO^{2-}$, $N\text{-}NO^{3-}$, $N\text{-}NH^{4+}$, $P\text{-}PO_4^{3-}$, and chloride.

2.5. Deionization mass balance in RDI

The mass balances of the following chemical compounds in the RDI were performed: nitrogen ions (NH^{4+}, NO^{3-}, and NO^{2-}) and orthophosphate. The variables considered in the mass balances were flow rate (Q), treatment time (T), and concentration (C) of each component in their respective streams. The feedwater flow was divided into three subsystems: purification influent, reject, and system cleaning, generating the purified effluent (QP), reject (QR), and system cleaning (QL) streams for each evaluated component. After determining the mass of each component in all system streams, STAN version 2.6 was used to create Sankey diagrams for the mass balance of each evaluated component. Mass balance calculations were performed for the operational scenarios with the highest specific removal efficiencies of each ion (Table 4). Thus, the following scenarios were selected:

- Ammonium, nitrate, and orthophosphate removal: repetition 1 of scenario 1.
- Nitrite removal: repetition 1 of scenario 4.

The mass flows at the system inlet and outlet were subdivided into:

- Inlet: purification influent, reject influent, and system cleaning influent (tertiary effluent).
- Outlet: purified effluent (after ion adsorption), reject effluent (after ion desorption), and cleaning effluent (ion adsorption).

Table 4 - Operational and performance conditions considered for mass balance calculations

PHASE 1 - REPETITION 1				
	TERTIARY EFFLUENT	PURIFICATION	REJECT	SYSTEM CLEANING
Flow rate ($L.min^{-1}$)	-	5.9	5.6	5.8
Time (min)	-	9.4	3.0	1.0
$N\text{-}NH_4^+$ (mg $N.L^{-1}$)	34.0	2.1	11.2	26.0
$N\text{-}NO_3^-$ (mg $N.L^{-1}$)	2.0	0.0	1.9	5.2
$P\text{-}PO_4^{3-}$ (mg $P.L^{-1}$)	1.3	0.3	0.4	0.7
PHASE 4 - REPETITION 1				
	TERTIARY EFFLUENT	PURIFICATION	REJECT	SYSTEM CLEANING
Flow rate ($L.min^{-1}$)	-	8.0	6.0	5.9
Time (min)	-	7.0	3.0	1.0
$N\text{-}NO_2^-$ (mg $N.L^{-1}$)	3.2	0.2	0.8	1.1

The mass of cleaning influent (inlet to the system) refers to the mass of residual ions that the cleaning step of the RDI failed to remove in the previous treatment cycle. Its mass was calculated using equations 6 to 11, and the results are shown in Figure 11. Therefore, the subsequent treatment cycle, starting with the purification step, begins with the presence of adsorbed ions on the electrodes of the equipment. In the case of the first repetition of the treatment cycle (as in the conditions analyzed below), the mass of the system cleaning step was considered, which was always performed when the RDI equipment was started. It is important to note that part of the mass retained in the RDI after the completion of the full treatment cycle remained in the system even after the rejection step. In other words, even after the ion desorption process, some ions remained on the electrodes. The global mass balance equation used was:

$$M_{\text{Purification } influent} + M_{\text{Reject influent}} + M_{\text{Cleaning influent}} = M_{\text{Purification effluent}} + M_{\text{Reject effluent}} + M_{\text{Cleaning effluent}} + M_{\text{Generated}} - M_{\text{Removed}} \quad (5)$$

The mass of each component in its respective stream was determined using the following equations:

$$M_{\text{Purification } influent} = C_{inf} \times Q_P \times T_P \quad (6)$$

$$M_{\text{Reject } influent} = C_{inf} \times Q_R \times T_R \quad (7)$$

$$M_{\text{Cleaning}\,influent} = C_{inf} \times Q_C \times T_C \quad (8)$$
$$M_{\text{Purification}\,effluent} = C_P \times Q_P \times T_P \quad (9)$$
$$M_{\text{Reject}\,effluent} = C_R \times Q_R \times T_R \quad (10)$$
$$M_{\text{Cleaning}\,effluent} = C_c \times Q_C \times T_C \quad (11)$$

Where:
Cinf - concentration in the feed influent ($mg.L^{-1}$);
CP - concentration in the purified effluent ($mg.L^{-1}$);
CR - concentration in the reject effluent ($mg.L^{-1}$);
CC - concentration in the system cleaning effluent ($mg.L^{-1}$);
QP - flow rate during the purification stage ($L.min^{-1}$);
QR - flow rate during the reject stage ($L.min^{-1}$);
QC - flow rate during the system cleaning stage ($L.min^{-1}$);
TP - time lapse of the purification stage (min);
TR - time lapse of the reject stage (min);
TC - time lapse of the system cleaning stage (min);
$M_{Purification\ influent}$ - mass of the evaluated component in the purification influent (mg);
$M_{Reject\ influent}$ - mass of the evaluated component in the reject influent (mg);
$M_{Cleaning\ influent}$ - mass of the evaluated component in the system cleaning influent (mg);
$M_{Purification\ effluent}$ - mass of the evaluated component in the purified effluent (mg);
$M_{Reject\ effluent}$ - mass of the evaluated component in the reject effluent (mg);
$M_{Cleaning\ effluent}$ - mass of the evaluated component in the system cleaning effluent (mg);
$M_{Generated}$ - mass of the generated component by the system (mg);
$M_{Removed}$ - mass of the removed component by the system (mg).

2.6. Statistical analysis of the results

The statistical analysis of the first experiment evaluated the influence of the combination of factor levels on the salinity removal efficiency of the equipment. Its factorial design (3 × 5) had a first factor referring to water recovery rates (70, 80, and 90%), and a second factor consisting of flow rates during the purification stage (6, 8, 10, 12, and 14 $L.min^{-1}$). In the second experiment, the removal of ionic compounds in the RDI was evaluated in five repetitions for all tested scenarios (6, 8, and 10 $L.min^{-1}$). To evaluate the impact of the factors on the response of interest, an analysis of variance (ANOVA) was performed. The assumptions of the models were checked by applying the Bartlett's test for homogeneity of variances and the Shapiro-Wilk test for normality. Comparisons between treatments were conducted using Tukey's test. All tests were conducted with a significance level of 95%.

3. RESULTS AND DISCUSSION

3.1. RDI desalination

The variation of effluent conductivity overtime during an operational cycle of RDI enabled the identification of four typical regions: (1) water purification (ion adsorption), (2) no hydraulic flow reject (ion desorption), (3) reject with the hydraulic flow, and (4) system cleaning (Figure 4).
During the purification stage, the fixed electrical voltage between the electrodes decreases the conductivity of the liquid to a minimum value that gradually increases afterward. At the same time, the electrical current decreases due to the gradual saturation of the capacitors operating with a constant electrical potential difference between them. Non-hydraulic flow reject stage reverses the electrical voltage at the electrodes, releasing the previously adsorbed ions into the spacer channel. However, they remain in the channel due to the absence of flow, as indicated by the relative stability of conductivity in the liquid phase. The operational configuration included this stage to prolong ion desorption time, increasing electrode regeneration without reducing water recovery rates. In the reject with hydraulic flow stage, the

concentrated effluent flows through the spacer channel, resulting in a temporary peak in conductivity. During the cleaning stage of the process, the washing of desorbed ions from the electrodes by continuous feeding with deionized water reduces conductivity in the effluent.

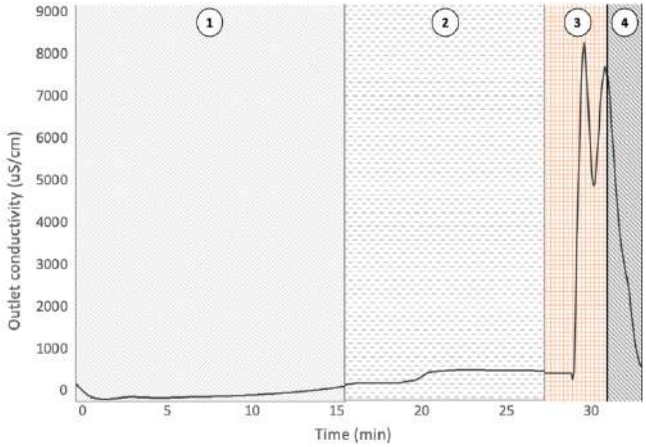

Figure 4 - Variation of effluent conductivity during a treatment cycle, with the purification (1), reject (2 and 3), and system cleaning stages (4).

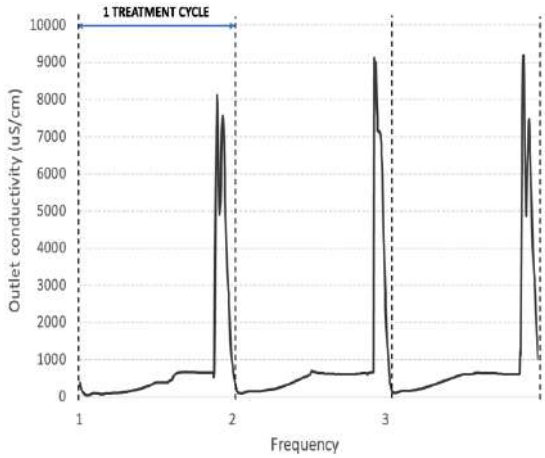

Figure 5 - Variation of conductivity in the RDI effluent over three subsequent treatment cycles.

The performance of the RDI in subsequent treatment cycles under the same operating conditions (hydraulic and electrical loads) indicates that electrosorption during the purification stage experiences a slight loss of efficiency (Figure 5). This suggests that the adopted operational strategy of capacitor rinsing during the reject cycle failed to completely regenerate the electrodes from one treatment cycle to another, resulting in an accumulation of charge in them over subsequent cycles.". The rejection stages also shows more pronounced conductivity peaks in the second and third repetitions, indicating the cumulative effect of charge retention by the electrodes throughout the treatment cycles.

3.2. Influence of water recovery rates on RDI performance

Lower water recovery rates resulted in lower conductivity values in the effluent of the purification stage (1) (Figures 6 and 7), evinced by the conductivity values obtained from the regeneration stage (2 and 3). It became evident that prolonging the purification stage decreased desalination efficiency due to electrode saturation during the ion adsorption stage. Electrosorption started to decline after about 10 minutes into the purification cycle, with the electrical conductivity of the effluent starting to increase. Tests with 90% water recovery rates significantly increased electrical conductivity in the CDI effluent, reaching values close to the conductivity of the process feed. The decrease in electrical current in the capacitors confirmed this observation, indicating that they were nearly saturated regarding their electrosorption capacity.

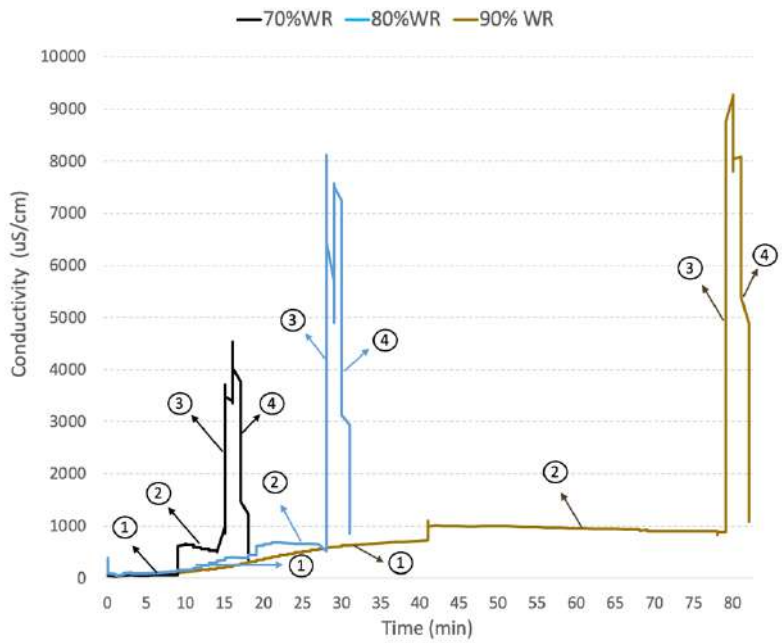

Figure 6 - Variation in conductivity as a function of water recovery rates in the purification (1), rejection (2 and 3), and RDI cleaning (4) stages.

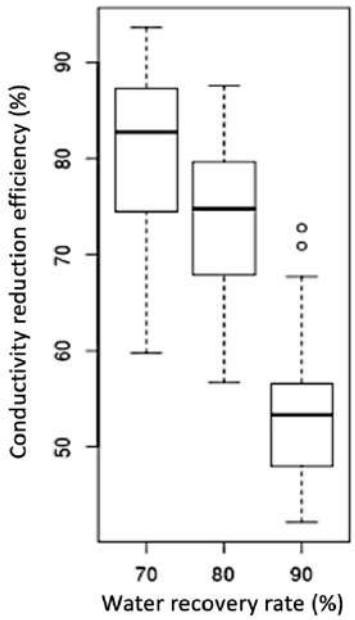

Figure 7 - Effect of water recovery rate on conductivity efficiency reduction.

3.3. Combined effects of hydraulic loading and water recovery rate in RDI

The strategy of varying the ionic load applied to the process during the experimental phases was implemented by varying the hydraulic loading (flow rate) (Table 5). As a general rule, increasing hydraulic loads tend to reduce desalination efficiency. The same occurs for the electrosorption time during the purification stage of the operational cycle, in which an increase leads to higher water recovery rates in the process. On the other hand, experimental phases with lower hydraulic loadings and water recovery rates better reduced wastewater conductivity efficiency, but with a higher specific energy consumption (Table 5 and Figure 8).

In Phase 1, characterized by a water recovery rate of 70%, hydraulic loading rate of 30.82 $m^3.m^{-2}.d^{-1}$, and an applied electric voltage of 5.3V showed the highest average conductivity reduction efficiency (92.8%). The desalinated effluent had an average conductivity of 69.80 µS/cm and a 2.17 $kWh.m^{-3}$ specific energy consumption. In Phase 7, under higher hydraulic loading and a water recovery rate of 70%, the RDI efficiency in reducing conductivity decreased to 83.2%, with a specific energy consumption of 1.25 $kWh.m^{-3}$. Lower desalination efficiencies (around 50 to 60%) occurred in tests with a water recovery rate of 90%, even when the hydraulic loading was low (e.g., Phase 3, hydraulic loading = 29.3 $m^3.m^{-2}.h^{-1}$, efficiency = 54.4%). The Tukey's test indicated that no significant difference in conductivity reduction efficiency between the approximate hydraulic loadings of 30.8 and 41.0 $m^3.m^{-2}.h^{-1}$,; 30.8 and 50.1 $m^3.m^{-2}.h^{-1}$; 41.0 and 50.1 $m^3.m^{-2}.h^{-1}$; and 60.4 and 69.5 $m^3.m^{-2}.h^{-1}$. The greatest difference occurred in tests with hydraulic loadings of 41.0 and 69.5 $m^3.m^{-2}.h^{-1}$, in which the removal efficiencies ranged from 7.6 to 26%.

Ramachandran et al. (2018) reported similar results, finding that the specific energy consumption of capacitive deionization increases proportionally with the amount of salt removed from the water. Regarding hydraulic loading, lower flow rates resulted in higher specific energy consumption. The combined impact of increased hydraulic loading and water recovery rate supports the findings of Hawks et al. (2018), who emphasize the need of carefully selecting operational parameters to avoid antagonistic effects on process performance.

Table 5 - Performance of RDI under greater hydraulic loading and water recovery rate

Phase	Flow Rate ($L.min^{-1}$)	Hydaulic Load ($m^3.m^{-2}.h^{-1}$)	Water Recovery Rate (%)	Voltage (V)	Conductivity (uS/cm)		Efficiency (%)	Specific Energy Consumption ($kWhr.m^{-3}$)
					Inlet	Outlet		
1	6.2	30.8	70	5.3	966	70	93	2.2
2	5.8	29.2	80	5.6	1287	267	79	3.0
3	5.9	29.3	90	5.9	1147	522	54	2.5
4	8.2	41.0	70	5.3	1040	160	85	1.7
5	8.1	40.6	80	5.6	1016	186	82	1.9
6	8.2	40.8	90	5.9	896	350	61	1.8
7	10.0	50.1	70	5.3	843	142	83	1.3
8	10.0	50.1	80	5.6	875	197	78	1.4
9	10.1	50.7	90	5.9	856	340	60	1.4
10	12.1	60.4	70	5.3	925	241	74	1.1
11	12.0	59.9	80	5.6	955	298	69	1.2
12	11.8	59.1	90	5.9	971	478	51	1.3
13	13.9	69.5	70	5.3	930	298	68	1.0
14	13.8	69.2	80	5.6	950	365	62	1.1
15	13.7	68.5	90	5.9	946	499	47	1.1

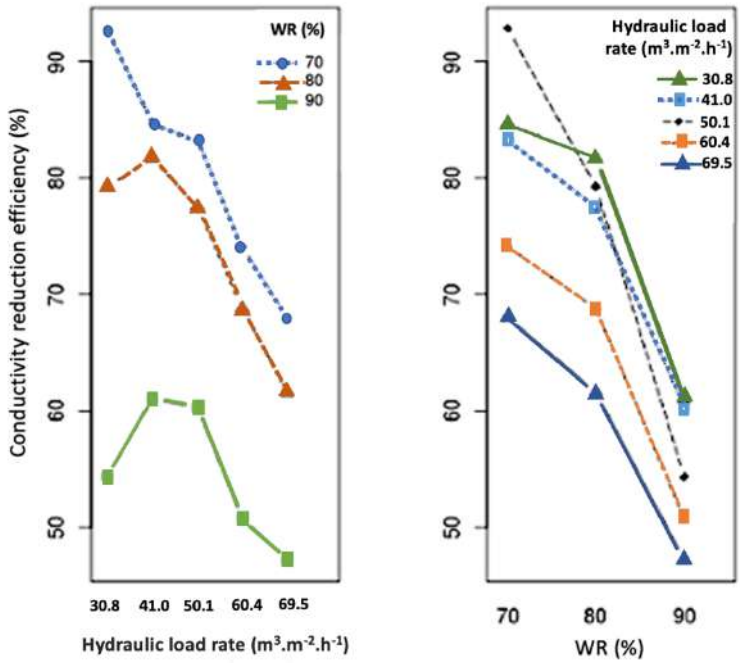

Figure 8 - Effects of the interaction between hydraulic loading (HLR) and water recovery rates (WR) on conductivity reduction efficiency

These results show no strong interaction between the two variables (HLR and WR) due to the apparent absence of an optimal combination that maximizes the efficiency of conductivity reduction. However, analysis of variance indicated that WR had the greatest influence on the variability of CDI efficiency, with the best results obtained in phase 1, followed by phases 4, 7, and 5. Out of 15 fifteen tested phases, six failed to meet the manufacturer's recommended operational requirements. They were unable to reduce the conductivity of the liquid stream to values equal to or lower than the conductivity of the feed water at the end of the system

cleaning step (ionic desorption). These phases (i.e., 2, 6, 10, 11, 13, and 14) were excluded from the selection process for the second round of testing.

One of the parameters used to assess the performance of CDI is ionic efficiency, defined as the ratio of moles of ions removed to moles of electrons used to charge the capacitor (Cohen et al., 2011). Since amperes represent coulombs per second, this value can be converted into moles per second and then compared to the rate of salt removal in moles per second. In theory, with monovalent species like NaCl, for each electron entering the cathode of the capacitor, an electron “place” is generated in the anode. The negative charge produced by the electron in the cathode attracts one sodium ion, while the place in the anode attracts one chloride ion. Consequently, one electron of current is capable of removing one monovalent dissolved molecule.

The voltage applied across the capacitor plays a pivotal role in both the short-term and long-term performance of the CDI process. Given that the desalination medium is water containing some salt content, the presence of H+ and OH- ions in the water, along with water hydrolysis, have significant impacts.

Analyzing the data gleaned from the first experimental phase (1st stage), it is apparent, as delineated in Table 5, that the ionic efficiency experiences a substantial decline as the voltage for the two-module system increases from 5.3VDC to 5.9VDC (or 2.65VDC to 2.95VDC per cell voltage). This phenomenon can be entirely attributed to the pronounced escalation of the hydrolysis reaction, or water splitting. The Nernst Potential represents the electrochemical cell potential for a given set of species. In the case of H+ and OH-, the theoretical potential for hydrolysis is 1.23VDC. However, this value is subject to numerous influencing factors, including competing reactions within a cell, a wide array of chemical species presents in water, changing concentrations of these species, and localized pH variations. In a standard capacitive deionization cell, the industry-recognized "safe" operating range, devoid of significant levels of hydrolysis, extends up to 2.2VDC per cell. Beyond this threshold, the rate of hydrolysis experiences an exponential surge until it becomes the predominant reaction, typically occurring at around 4.0VDC, which is the standard operating voltage for an industrial hydrolysis cell.

Table 5 - Variation of ionic efficiency as a function of the applied voltage to the RDI process.

Specific Flowrate ($ml/min/m^2$)	Voltage								
	5,3 VDC			5,6 VDC			5,9 VDC		
	IE %	Recovery %	Reduction %	IE %	Recovery %	Reduction %	IE %	Recovery %	Reduction %
294,5	24,8	70,0	92,0	9,1	80,0	71,7	2,6	90,4	79,4
404,8	35,3	71,0	82,5	18,3	80,5	78,4	5,0	90,8	55,0
500,7	48,1	71,0	79,4	25,6	80,7	74,7	7,6	90,8	53,3
596,0	61,7	70,9	66,5	33,2	80,5	64,5	10,1	90,4	46,7
687,0	67,4	70,2	59,7	36,4	80,1	56,7	12,2	90,5	44,9

Observations in this context reveal that the ionic efficiency displays an upward trend as the flow rate during the cleaning cycle increases. This phenomenon can be elucidated by considering the diminished molar load imposed on the cell at lower flow rates. This, in turn, results in lower concentrations of "non" H+ and OH- ions at the surface of the membrane/electrode, consequently reducing the inflated Nernst potential towards its theoretical value of 1.23VDC. As a result, this leads to an augmentation in the reaction rate of hydrolysis. Consequently, it can be inferred that as the operating voltage decreases, the ionic efficiency exhibits an ascending trajectory, accompanied by a concurrent reduction in power consumption. Other applications of the RDI process suggest that ionic efficiencies can exceed the 90% mark across all flow rates at approximately 4.8VDC or below 2.4VDC for a single cell.

If confirmed, it is expected that the voltage decreases and simultaneous increase in ionic efficiency will lead to a corresponding reduction in specific energy consumption (kWh/m^3) during desalination.

3.4. RDI removal of different ionic compounds

Under similar CDI operating conditions, the results obtained in this second stage of the research showed slightly lower desalination rates than the first stage. The conductivity reduction efficiencies in the second stage were 84.6, 77.1, and 74%, with outlet conductivity values of 185.4, 269.4, and 296.6 uS/cm (scenarios 1, 4, and 7), respectively (Table 6). The removal efficiencies of different ionic compounds in all test phases ranged from 84 to 74% (ammonium), 91 to 88% (nitrite), 100 to 73% (nitrate), and 61 to 42% (orthophosphate) (Table 6). The average concentrations in the treated effluents were, 8.2, and 7.4 mg $N.L^{-1}$ (ammonium); 0.05, 0.3, and 0.5 (nitrite); 0 mg, 0.4 mg, and 2.3 (nitrate); and 0.5, 0.9, and 1.1 mg $P.L^{-1}$ (orthophosphate) in phases 1, 4, and 7, respectively. Ammonium ion had the highest concentration at the RDI inlet and was removed in larger quantities than the others during the purification step. Despite this ammonium removal, increased hydraulic loading and a decrease in the removal efficiency of different ions of interest showed a direct relation that resembled the desalination stage in the previous research phase. Under a hydraulic loading of 50.1 $m^3.m^{-2}.h^{-1}$ (phase 7), orthophosphate had the lowest reduction, whereas nitrite had the highest reduction. A hydraulic loading of 30.8 $m^3.m^{-2}.h^{-1}$ (phase 1) showed the highest removal efficiencies for all analyzed compounds, performing the best for nitrate ions.

All tests showed a preferential electrosorption of nitrate ions over nitrite ions. This result can be attributed to the higher concentration of nitrate in the RDI inlet and its smaller ionic radius, as nitrite and nitrate ions have the same electrical charge (HASSANVAND et al., 2018). Several studies report that the ion with the highest concentration in solutions with different ion concentrations is removed in larger quantities. Ions with a higher charge are more easily adsorbed than ions with the same charge, and the selectivity of ion adsorption strongly depends on the atomic radius (Gamaethiralalage et al., 2021). Marcus (1991) and Hou; Huang (2013) also describe the individual influence of electrical charge and ionic radius of each ion, stating that electrosorption more easily remove divalent ions than monovalent ions. Following the same line of reasoning, the lower efficiencies of RDI in the removal of PO_4^{3-} ions stemmed from their low concentration in the feed and their larger ionic radius. Table 7 details the chemical properties of the ions evaluated in this research.

Furthermore, some studies describe that the combination of higher electrical charges and large ionic radii also negatively affects the penetration of ions into the electrode pores (LI; YANTING; STEWART; TANG, 2018; SAKAR et al., 2019). Capacitive deionization studies of solutions with various ions by Mubita et al. (2019) and Hawks et al. (2019) showed the prevalence of electrosorption of chloride ions (atomic radius of 0.181 nm) over divalent ions (sulfate, atomic radius of 0.230 nm). The same studies indicated a prevalence of nitrate ion adsorption over chloride and sulfate ions, highlighting the strong influence of electrode pore size and atomic radius on electrosorption selectivity. Finally, results indicate that the removal efficiencies of ammonium, nitrite, nitrate, and orthophosphate ions in RDI suffered the direct influence of the applied hydraulic loading. This stems from the shorter contact time of the solution with the electrodes and the higher mass load of ions applied to the process. These results support Villar et al. (2010), which state that the amount of ions adsorbed by the electrodes proportionally increases to their concentration in the feed solution.

Table 6 - Composition of the tertiary effluent and purified water stream generated after passing through the RDI in phases 1, 4, and 7 (n=5)

PARAMETERS	TERTIARY EFFLUENT	PURIFIED - PHASE 1				AVERAGE EFFICIENCY	TERTIARY EFFLUENT	PURIFIED - PHASE 4				AVERAGE EFFICIENCY	TERTIARY EFFLUENT	PURIFIED - PHASE 7				AVERAGE EFFICIENCY
		Median (SD)	Minimum	Maximum	CV			Median (SD)	Minimum	Maximum	CV			Median (SD)	Minimum	Maximum	CV	
Temperature (°C)	23.8	24.6 ± 0.2	24.3	24.8	1%	0%	24.0	25.0 ± 0.1	24.8	25.1	0%	0%	24.3	25.3 ± 0.3	25.1	25.7	1%	0%
pH	7.6	7.0 ± 0.4	6.4	7.5	6%	8%	7.7	7.5 ± 0.1	7.4	7.7	1%	2%	7.6	6.8 ± 0.1	6.7	6.9	1%	10%
Turbidity (NTU)	0.6	0.4 ± 0.1	0.4	0.5	14%	29%	0.7	0.4 ± 0.1	0.3	0.5	13%	46%	0.5	0.4 ± 0.1	0.3	0.7	30%	7%
Conductivity (uS/cm)	1097	185.4 ± 57.5	109	240	31%	85%	1056	269.4 ± 79.3	140	332	29%	77%	1076	296.6 ± 87.4	162	388	29%	74%
TDS (ppm)	547	93.0 ± 28.5	55	120	31%	83%	528	134.8 ± 39.3	71	166	29%	75%	538	148.4 ± 43.7	81	194	29%	72%
OD ($mg.L^{-1}$)	5.1	3.7 ± 0.7	2.8	4.6	18%	28%	4.5	3.5 ± 0.5	2.7	3.9	15%	23%	4.6	4.8 ± 0.9	3.4	5.9	19%	0%
COD ($mg\ O_2 L^{-1}$)	41	29.8 ± 3.6	25	33	12%	27%	25	19.1 ± 2.1	16	21	11%	23%	32	19.2 ± 6.0	14	26	31%	40%
Total Alkalinity	176	32.0 ± 12.6	14	44	39%	82%	176	52.4 ± 16.7	24	66	32%	70%	146	47.6 ± 34.2	0	78	72%	67%
$N\text{-}NH_4^+$ ($mg\ N.L^{-1}$)	34.0	5.5 ± 2.4	2.1	7.6	43%	84%	32.3	8.2 ± 3.2	2.9	10.5	39%	75%	28.1	7.4 ± 3.2	2.5	10.4	43%	74%
$N\text{-}NO_2^-$ ($mg\ N.L^{-1}$)	0.6	0.1 ± 0.01	0	0.1	20%	91%	3.2	0.3 ± 0.1	0.2	0.4	25%	91%	4.1	0.5 ± 0.1	0.4	0.7	24%	88%
$N\text{-}NO_3^-$ ($mg\ N.L^{-1}$)	2.0	0	0	0	0%	100%	7.6	0.4 ± 0.3	0.1	0.7	83%	95%	8.6	2.3 ± 0.7	1.6	3.3	29%	73%
$P\text{-}PO_4^{3-}$ ($mg\ P.L^{-1}$)	1.3	0.5 ± 0.2	0.3	0.7	36%	61%	1.8	0.9 ± 0.2	0.6	1.0	19%	53%	1.9	1.1 ± 0.3	0.7	1.3	25%	42%
Cl^- ($mg.L^{-1}$)	154.3	9.3	-	-	-	94%	145.0	14.7	-	-	-	90%	148.4	16.7	-	-	-	89%

Table 7 - Chemical properties of the evaluated ionic compounds

PARAMETERS	CHARGE	IONIC RADIUS (nm)
$N\text{-}NH_4^+$	+ 1	0.148
$N\text{-}NO_2^-$	-1	0.192
$N\text{-}NO_3^-$	-1	0.179
$P\text{-}PO_4^{3-}$	-3	0.238

Source: Adapted from Marcus (1991)

3.5. Mass balance of deionization in RDI

Repetition 1 of phase 1 obtained the best result for ammonium removal in this second stage of this research, characterized by low hydraulic load applied during the purification stage, a lower water recovery rate, and a reduction in ion accumulation on the electrodes throughout subsequent treatment cycles. Mass and energy balances resulted in a removed mass of 1211.73 mg and an energy consumption of 1.5 kWh in the complete cycle. By relating both, energy density totaled 47.0 $kWh.kg^{-1}$ $N\text{-}NH^{4+}$ for every removed kilogram (Figure 11a). On the other hand, the retained mass of orthophosphate, which had lower concentrations at the RDI inlet and a larger atomic radius, was the lowest among the ions of interest (36.38 mg) (Figure 11d), with its energy density reaching a maximum value of 1531.84 $kWh.kg^{-1}$ P. This may be a consequence of the amount of mass adsorbed during the purification stage, associated with a very short subsequent rejection stage, retaining ions inside the RDI at the end of the treatment cycle. Despite the electrode regeneration stage, some ions remain trapped in their pores, as described earlier. Nitrate ions show a negative mass, meaning that the mass contained in the output stream is greater than in the input, indicating that the system produces mass. A hypothesis for this occurrence attributes this to possible reading errors in the flow measurement equipment or the quantification of the evaluated component concentrations.

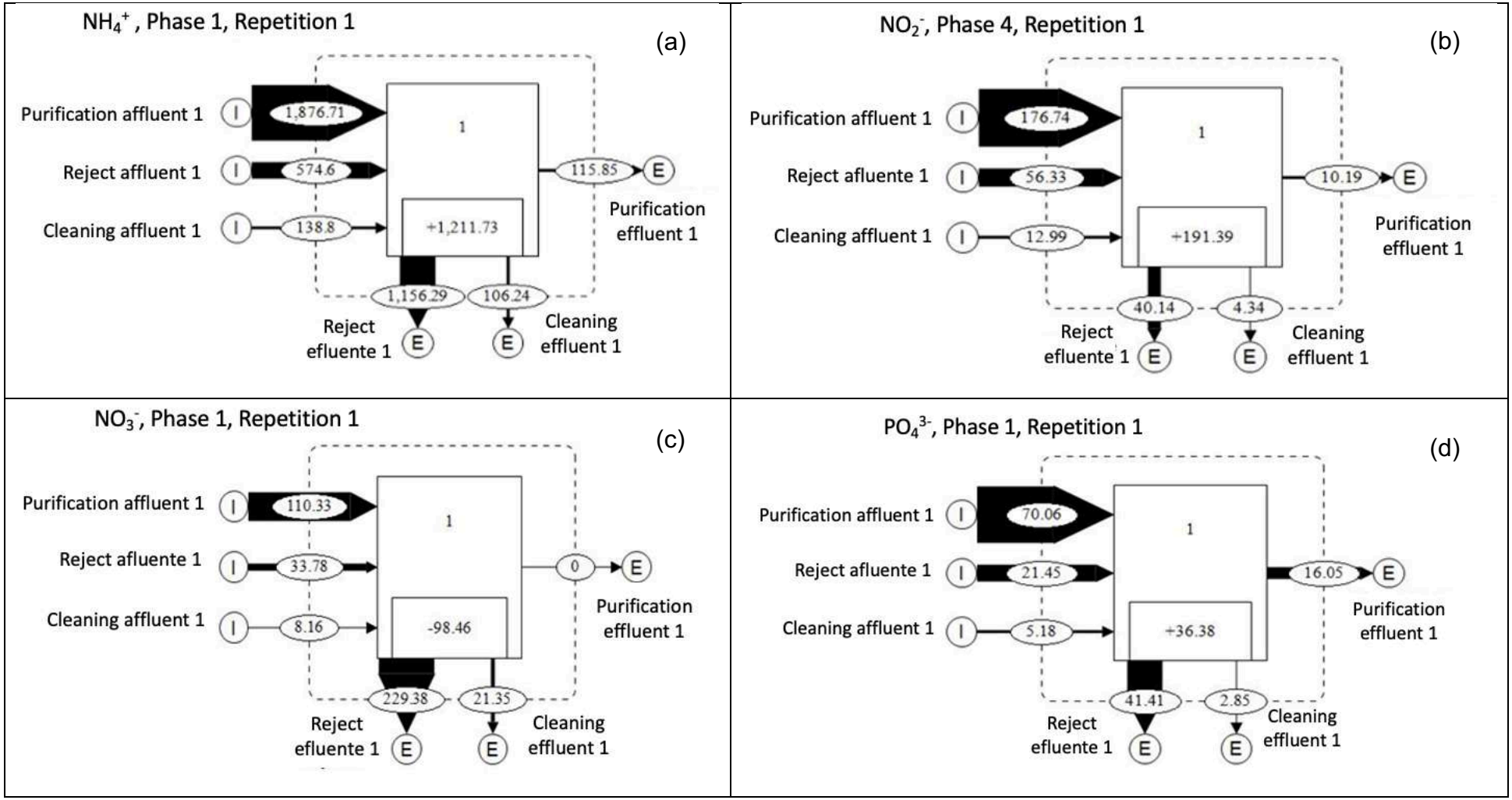

Figure 11 - Sankey diagram of the mass balance for ammonium (in mg N) (scenario 1); nitrite (in mg N) (scenario 4); nitrate (in mg N) (scenario 1); and orthophosphate ions (in mg P) (scenario 1).

4. CONCLUSION

Under the imposed operational conditions, radial capacitive deionization (RDI) showed a high potential toward desalination, reducing conductivity efficiency up to 92.8% and consuming 2.17 $kWh.m^{-3}$ of specific energy. It also efficiently removed ammonium, nitrite, nitrate, and orthophosphate ions, with average efficiencies of up to 84, 91.4, 100, and 60.5, respectively. However, a significant loss of efficiency occurred when the process operated continuously due to the accumulation of mass within the process over subsequent treatment cycles. Lower hydraulic loads resulted in better RDI ion removal from wastewater but with higher specific energy consumption. Higher rates of treated water recovery led to lower ion removal efficiencies and energy consumption. The ion desorption (reject) stage configured the limiting factor for performance, requiring proper adjustment of time lapse, flow rate, and applied electric voltage to ensure efficient ion adsorption in the subsequent purification stage. Due to its level of sophistication, this process requires a precise selection of operational parameters, especially to treat waters with a wide range of ionic compounds. Additionally, the long-term performance of the process under continuous operation still requires further, more detailed investigations.

ACKNOWLEDGMENTS

The authors would like to express their gratitude to the FORTLEV, ATLANTIS, and FLUXO companies for their material and logistical support in the construction and monitoring of the pilot system. They also extend their thanks to CESAN and AEGEA for their logistical support during the experiments.

CREDIT AUTHORSHIP CONTRIBUTION STATEMENT

Ricardo Franci Gonçalves: Conceptualization, Research, Writing - Elaboration of the original draft, Writing - Review & Edition, Constansa Valadares Tripoli: Conceptualization, Research, Writing - Elaboration of the original draft, Writing - Review & Edition. Patrick Curran: Writing & Review.

DECLARATION OF COMPETING INTEREST

The authors declare that they have no known competing financial interests or personal relationships that could have appeared to influence the work reported in this paper.

DATA AVAILABILITY STATEMENT

The datasets generated during and/or analyzed during the current study are available from the corresponding author on reasonable request.

REFERENCES

APHA. **Standard Methods for the Examination of Water and Wastewater**. American Public Health Association, Washington, DC (2012).

Chai, S.; Xi, J.; Chen, L.; He, W.; Shen, J.; Gong, H. Selective Ion Removal by Capacitive Deionization (CDI)-Based Technologies. Processes (2022).

Cohen, I., Avraham, E., Noked, M., Soffer,, A., Aurbach, D. Enhanced Charge Efficiency in Capacitive Deionization Achieved by Surface-Treated Electrodes and by Means of a Third Electrode. **The Journal of Physical Chemistry C** (2011).

CHEN, Z. et al. A study of electrosorption selectivity of anions by activated carbon electrodes in capacitive deionization. **Desalination** (2015) v. 369, p. 46–50.

CHUNG, T-C. Evaluating the desalination performance and efficiency of capacitive deionization with activated carbon electrodes. Dissertation (Master), **University of Toronto**, (2018) 154p.

DEMIRER, O. N. et al. Energetic performance optimization of a capacitive deionization system operating with transient cycles and brackish water. **Desalination** (2013) v. 314, p. 130–138.

Guyes, E.N., Shocron, A.N., Chen, Y. *et al.* Long-lasting, monovalent-selective capacitive deionization electrodes. *npj* ***Clean Water*** **4** (2021) 22.

HASSANVAND, A. et al. A comparison of multicomponent electrosorption in capacitive deionization and membrane capacitive deionization. **Water Research** (2018) v. 131, p. 100– 109.

HAWKS, S. A. et al. Performance Metrics for the Objective Assessment of Capacitive Deionization Systems. **Water Research** (2018).

HAWKS, S. A. et al. Using Ultramicroporous Carbon for the Selective Removal of Nitrate with Capacitive Deionization. **Environmental Science and Technology**, v. 53, n. 18, p. 10863–10870, 2019.

HOU, C.; HUANG, C. A comparative study of electrosorption selectivity of ions by activated carbon electrodes in capacitive deionization. **Desalination** (2019) v. 314, p. 124– 129.

HUYSKENS, C; HELSEN, J; HAAN, A B De. Capacitive deionization for water treatment: Screening of key performance parameters and comparison of performance for different ions. **Desalination** (2013) v. 328, p. 8–16.

J.G. Gamaethiralalage, K. Singh, S. Sahin, J. Yoon, M. Elimelech, M.E. Suss, P. Liang P.M. Biesheuvel, R.L. Zornitta, L.C.P.M. de Smet. Recent advances in ion selectivity with capacitive deionization. **Energy Environ. Sci.,** (14) (2021), pp. 1095-1120

LI, Y. et al. Effects of the hydration ratio on the electrosorption selectivity of ions during capacitive deionization. **Desalination** (2016) v. 399, p. 171–177.

LI, Y.; STEWART, T. C.; TANG, H. L. A comparative study on electrosorptive rates of metal ions in capacitive deionization. **Journal of Water Process Engineering (**2018), v. 26, n. April, p. 257–263.

MAHESHWARI, K.; AGARWAL, M.; SOLANKI, Y. S. Electrode material effect on electrochemical characterization, properties, and operational parameters in capacitive deionization. **Materials Today: Proceedings** (2020), n. 10.1016.

MARCUS, Y. **Thermodynamics of Solvation of Ions**. v. 87, n. 18, p. 2995–2999, 1991.
MUBITA, T. M. et al. Selective adsorption of nitrate over chloride in microporous carbons. **Water Research** (2019) v. 164, p. 114885.

NOKED, M et al. Assessing the Concentration Effect on Hydration Radii in Aqueous Solutions by Electroadsorption on a Carbon Molecular Sieve Electrode. **The Journal of Physical Chemistry C** 114 (31) (2010) 13354–13361.

PORADA, S. et al. Effect of electrode thickness variation on operation of capacitive deionization. **Electrochimica Acta** (2012) v. 75, p. 148–156.

RAMACHANDRAN, A. et al. Frequency analysis and resonant operation for efficient capacitive deionization. **Water Research** (2018) v. 144, p. 581–591.

RAMACHANDRAN, A. et al. High water recovery and improved thermodynamic efficiency for capacitive deionization using variable flowrate operation. **Water Research** (2019) v. 155, p. 76–85.

Rommerskirchen, A; Linnartz, C; Egidi, F; Kendir, S; Wessling, M. Flow-electrode capacitive deionization enables continuous and energy-efficient brine concentration. ***Desalination*** (2022).

SAKAR, H. et al. Ammonium removal and recovery from real digestate wastewater by a modified operational method of membrane capacitive deionization unit. **Journal of Cleaner Production** (2019) v. 215, p. 1415–1423. https://doi.org/10.1016/j.jclepro.2019.01.165

Salari K, Zarafshan P, Khashehchi M, Chegini G, Etezadi H, Karami H, Szulżyk-Cieplak J, Łagód G. Knowledge and Technology Used in Capacitive Deionization of Water. **Membranes** (2022).

SHUI, P.; ALHSEINAT, E. Quantitative insight into the effect of ions size and electrodes pores on capacitive deionization performance. **Electrochimica Acta** (2019) p. 135176.

SUSS, M. E. et al. Water desalination via capacitive deionization: What is it and what can we expect from it? **Energy and Environmental Science** (2015) v. 8, n. 8, p. 2296–2319.

TANG, W.; KOVALSKY, P.; HE, D.; WAITE, T.D., Fluoride and nitrate removal from brackish groundwaters by batch-mode capacitive deionization, **Water Research** (2015).

TSAI, S.et al. Exploring the electrosorption selectivity of nitrate over chloride in capacitive deionization (CDI) and membrane capacitive deionization (MCDI). **Desalination** (2021) v. 497, n. 1, p. 114764.

VILLAR, I. et al. Capacitive deionization of NaCl solutions with modified activated carbon electrodes. **Energy and Fuels** (2010) v. 24, n. 6, p. 3329–3333.

Zhang C, Wu L, Ma J, et al. Evaluation of long-term performance of a continuously operated flow-electrode CDI system for salt removal from brackish waters. **Water Research** (2020).